Journal of Solid State Chemistry 183 (2010) 2662–2668

Contents lists available at ScienceDirect

Journal of Solid State Chemistry

journal homepage: www.elsevier.com/locate/jssc

Nitrogen vacancy and ferromagnetism in Cr-doped GaN: First-principles calculations

Yanlu Li [a], Weiliu Fan [b,*], Honggang Sun [a], Xiufeng Cheng [a], Pan Li [a], Xian Zhao [a,*], Minhua Jiang [a]

[a] State Key Laboratory of Crystal Materials, Shandong University, Jinan 250100, China
[b] School of Chemistry and Chemical Engineering, Shandong University, Jinan 250100, China

ARTICLE INFO

Article history:
Received 5 May 2010
Received in revised form
27 August 2010
Accepted 30 August 2010
Available online 15 September 2010

Keywords:
GaN
Cr-doped
Nitrogen vacancy
Ferromagnetism
First-principles calculation

ABSTRACT

Nitrogen defects and their effect on the ferromagnetism (FM) in Cr-doped GaN have been systematically investigated by first-principles. Four considered configurations including one N vacancy (V_N), single substitutional Cr, double substitutional Cr, and complex of Cr–V_N are all ferromagnetic. The lowest energy arrangements for double Cr-doped (or Cr–V_N) GaN occur at the nearest Cr–Cr (or Cr–V_N) distance. One Cr contributes 84.3% of the total magnetic moment (2.533 μ_B), while one Cr–Cr pair leads to 5.998 μ_B moment (more than twice moment of one Cr) by the strong d–d spin coupling, which is mediated by two Cr 3d states antiferromagnetically coupling with the "commonly shared" N 2p states, and driven by a double exchange mechanism. The V_N can enhance the FM by adding about 1 μ_B to the Cr moment but reduce the FM spin exchange interaction between the nearest Cr–Cr pairs, so experimentally, high-performance samples may be synthesized by controlling N pressure.

1. Introduction

Dilute magnetic semiconductor (DMS) materials have become a topic of great current interest because both the charge, arising out of the s and p electrons of the semiconductor, and spin, arising out of the magnetic impurity, can be used in novel spintronics devices [1,2]. The interest in the family of DMSs started with the discovery of ferromagnetism in Mn-doped InAs and GaAs with a Curie point (T_c) of 110 K [1]. However, it is required to fabricate a high-T_c ferromagnet as a first step towards a practical application of DMSs for semiconductor spintronics [3].

Group III-nitride semiconductors doped with 3d transition-metal (TM) such as Mn or Cr show ferromagnetism with high Curie temperature, and their band structures are much more suitable for spin injection than those of TMs-doped GaAs [4]. Among the III-nitride semiconductors, GaN, with wide band gap energy of 3.39 eV, has been one of the most promising materials for information processing with short wavelength optics [5,6]. Therefore, detailed investigation of the ferromagnetism of GaN-based DMSs is of great importance. Considering that the binding energy of Cr-doping in GaN is larger than that of Mn, it may be possible to dope the GaN with Cr more easily than with Mn. Thus, the Cr-doped GaN could prove to be a robust system for applications. Currently, many meaningful works have been carried out in the Cr-doped GaN DMSs [7–15]. Especially, a discovery [15] reported a high Curie temperature above 900 K for the Cr-doped GaN sample, and such high Curie temperatures make the materials promising for practical spintronic applications. In that work, Liu et al. pointed out that most of the Cr impurities are located on substitutional sites.

The ferromagnetism in Cr-doped GaN should be attributed to p–d hybridization of N 2p and Cr 3d states. On the other hand, defects and impurities are believed to play important roles in DMSs of wide semiconductor gaps. It has been argued before that among the native defects (vacancies, interstitials, and antisites) only Ga vacancies are assumed to appear in observable amounts in as-grown GaN [16–23]. Contrary to the earlier expectations, a recent theoretical study [24] confirmed that the nitrogen vacancy should be the dominant defect in GaN in the whole range of Fermi-level positions in the band gap. In order to gain insight into the effects of the impurities, it is highly desirable to investigate the effect of N vacancy on the high-temperature ferromagnetism in Cr-doped GaN materials, and in return its elucidation is helpful to obtain deeper insight into the essential mechanism of the high-temperature ferromagnetism. In other word, we can say that vacancies are quite common in many crystals, both in closed-packed metallic structures as well as in open covalent structures [25].

In this paper, we performed a detailed first-principles investigation of Cr-doped GaN with N defects, with the goal of identifying the origin of ferromagnetism and the effects of N defects on the magnetic behavior. First, the atomic positions and

* Corresponding authors. Fax: 86 531 88365174.
E-mail addresses: fwl@sdu.edu.cn (W. Fan), zhaoxian@icm.sdu.edu.cn (X. Zhao).

0022-4596/$ - see front matter © 2010 Elsevier Inc. All rights reserved.
doi:10.1016/j.jssc.2010.08.038

the unit-cell parameters were allowed to relax to the minimum energy configuration to investigate six kinds of configurations of $CrGa_{35}N_{36}$ (one substitutional Cr atom), $Ga_{36}N_{35}$ (one V_N), $Cr_2Ga_{34}N_{36}$ (two substitutional Cr atoms), $CrGa_{35}N_{35}$ (one substitutional Cr atom and one V_N), $CrGa_{35}N_{36}+N_O$ (one substitutional Cr atom with one octahedral intersititial N), and $CrGa_{35}N_{36}+N_T$ (one substitutional Cr atom with one tetrahedral intersititial N). Then, via calculating the defect formation energies, we chose the most stable structures of the former four kinds of configurations to study their electronic properties and magnetism interactions to identify the origin of ferromagnetism as well as the difference in the electronic structures and magnetism under different impurity concentrations and N defect condition. We also aimed to find the trend of proper N partial pressure to synthesize Cr-doped GaN DMSs with high ferromagnetism.

2. Computational details

All the structure optimizations and total energy spin-polarized DFT calculations have been performed by using the program package DMol^3 code [26], in which wave functions are expanded in terms of accurate numerical basis sets. All electron Kohn–Sham wave functions are expanded in a Double Numerical basis with Polarized orbital (DNP) basis set [26]. A fine real-space cutoff of 4.8 Å and a generalized gradient approximation (GGA) for the exchange correlation energy functional as parametrized by Perdew–Wang (PW91) [27] are used. The Brillouin-zone integrations are performed with the special k point method over a $3\times3\times2$ Monkhorst-Pack mesh [28]. The convergence criteria for structure optimization and energy calculation were set to fine quality making the tolerance for self-consistent field (SCF), energy, maximum force, and maximum displacement to be 1.0×10^{-6} hartree/atom, 1.0×10^{-5} hartree/atom, 0.002 hartree/Å, and 0.005 Å (1 hartree=27.21 eV), respectively. We have first performed a geometry optimization for the lattice constants of the pure structure. The calculated equilibrium structural parameters of GaN ($a=b=3.226$ Å, $c=5.257$ Å) are in good agreement with the experimental values [29] with deviations within 2%, which indicates that the calculated parameters in our calculations are reliable and reasonable. On the basis of equilibrium lattice constants of GaN, we establish the supercells with impurities and defect, and relax them to the minimum energy configurations. All the electronic structures and magnetic moments are calculated on the corresponding optimized crystal geometries.

We used $3\times3\times2$ GaN supercells containing 72 atoms to study the wurtzite GaN with doped Cr atoms and N defects (including both nitrogen vacancies and nitrogen interstitials), as shown in Fig. 1. Some of the Ga and N atoms are numbered to facilitate our discussion as we replace various Ga sites by Cr and remove some N sites. We substitute a Cr atom for a Ga atom to form a supercell consisted of one Cr atom, 35 Ga atoms and 36 N atoms, amounting to 1.39% Cr doping concentration, and this first substituting Cr atom is named as Cr0. The second Cr atom is introduced by substituting a Cr atom, for example, for the Ga atom labeled as Ga1 in Fig. 1 to form the Cr0–Cr1 pair in the supercell. Similarly, by removing one N atom, such as the one labeled as N1 in Fig. 1a, a nitrogen vacancy V_{N1} is created in the supercell. An octahedral N interstitial N_O atom is introduced by adding one N atom at an octahedral site, which is located at the center of the hexagonal channel of the supercell, and a tetrahedral N interstitial N_T atom is obtained by adding one N atom at a tetrahedral site, which corresponds to the center of the line joining the closest nonbonded Ga and N atoms along the z-axis.

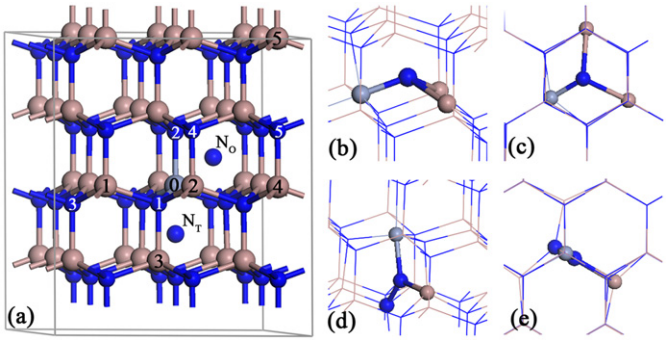

Fig. 1. (a) Schematic structure of Cr-substituted $3\times3\times2$ wurtzite GaN supercell $CrGa_{35}N_{36}$. The cyan, brown and blue balls represent the Cr, Ga and N atoms, respectively. The second substituted-Cr atom and the N vacancy locate at the Ga sites and N sites labeled as 1–5, respectively. The interstitial N atom at the octahedral and tetrahedral sites are also marked as N_O and N_T. (b, d) Side-view and (c, e) top-view of the partial geometric structure of Cr-doped with N_O (b, c) and N_T (d, e) respectively. (For interpretation of the references to color in this figure legend, the reader is referred to the web version of this article.)

3. Results and discussions

3.1. Optimized structures and defect formation energies

It has been theoretically reported earlier that the TM atom prefers the substitutional site than the interstitial site in the host GaN [30]. Wang et al. [31] observed temperature-dependent photoluminescence spectra of Cr-implanted GaN, which imply that Cr substitutionally incorporates on the Ga site and forms a deep acceptor level in GaN. Therefore, the lattice structures and internal atomic positions are fully optimized for N vacancy ($Ga_{36}N_{36}+V_N=Ga_{36}N_{35}$), Cr-doped GaN ($CrGa_{35}N_{36}$), two Cr-doped GaN ($Cr_2Ga_{34}N_{36}$), Cr atom with N vacancy ($CrGa_{35}N_{36}+V_N=CrGa_{35}N_{35}$), Cr atom with octahedral N interstitial ($CrGa_{35}N_{36}+N_O$), and Cr atom with tetrahedral N interstitial ($CrGa_{35}N_{36}+N_T$). Because it is a priori not clear which Ga sites would be replaced by Cr and which N sites would be removed, various atomic configurations for pairs of Cr–Cr, Cr–V_N, Cr–N_O, and Cr–N_T with different distances have been studied. For $Cr_2Ga_{34}N_{36}$, we calculated the total energies of the ferromagnetic (FM) and antiferromagnetic (AFM) states of each configuration, and the changes of the relative total energies are plotted in Fig. 2. As for the case of FM orientation, the total energy changes with the different Cr–Cr distances, and the lowest total energy is achieved when the two Cr atoms (Cr0–Cr1) are in the same layer and have the nearest distance (connected with the same N atom). The antiferromagnetic orientation has the similar trend, while the lowest energy is reached at the nearest Cr0–Cr3 configuration. The ferromagnetic orientation is lower in total energy by 288, 171 and 26 meV than the corresponding antiferromagnetic ones for Cr0–Cr1 (Cr0–Cr2), Cr0–Cr3, and Cr0–Cr4, respectively. And when the two Cr atoms are in the farthest sites (Cr0–Cr5), the total energies of ferromagnetic and antiferromagnetic ones are almost the same. We also give the variation of relative total energy with the distance for $Ga_{36}N_{36}+V_N$ in Fig. 2. The total energy also becomes larger with the increase of the distance between Cr and V_N, and the system has the lowest total energy when Cr and V_N are the nearest neighbors (Cr0–V_{N1}). For one Cr doping with an interstitial N atoms, the most stable structures can be found when Cr and N_i has the nearest distance, and the optimized structures containing an octahedral and tetrahedral N atom are shown in Fig. 1b–d.

We further calculate the formation energies (E_f) for all the four cases by assuming the Cr and Ga atom reservoirs are bulk Cr

and bulk Ga, thus

$$E_f = E_{Cr/V_N} - E_{GaN} - n\mu_{Cr} + m\mu_{Ga} + \frac{l}{2}E_{N_2} + n_N\mu_N,$$

where E_{Cr/V_N}, E_{GaN}, and E_{N_2} are the total energy of GaN with Cr impurity or/and N vacancy, pure GaN, and N_2, respectively. μ_{Cr}, μ_{Ga}, and μ_N are the atom chemical potentials of Cr, Ga and N. The integers n, m, l are the number of doped Cr atoms and substituted Ga and N atoms, respectively. Variation of the chemical potentials in the equation is equivalent to varying the nitrogen partial pressure experimentally. The nitrogen-rich limit occurs when μ_N is equal to the chemical potential of nitrogen in N_2 (0 eV). The nitrogen-poor limit is defined when μ_N is from the thermodynamical stability of GaN ($\mu_N+\mu_{Ga}=\mu_{GaN}$). The calculated formation energies for the six lowest energy structures are listed in Table 1. We find that in both N-rich and N-poor conditions the N vacancy is easy to form, which is consistent with the experimental condition. The formation energy of single Cr-doped GaN supercell is 1.7 eV while that of double Cr-doped GaN supercell is larger, indicating that the substitutional dopant becomes much harder with the increasing of doping concentration. In the case of $CrGa_{35}N_{36}+V_N$, the formation energy is much higher, especially for the N-rich condition, implying that in the real samples it is helpful to obtain Cr-doped GaN dilute magnetic semiconductor in the N-poor condition. Besides, the formation energies of $Cr+N_O$ (and N_T) are much too high as compared to the other doping systems, even in the N-poor condition, to exist in the real samples, and therefore the related analysis of interstitial cases are not presented here.

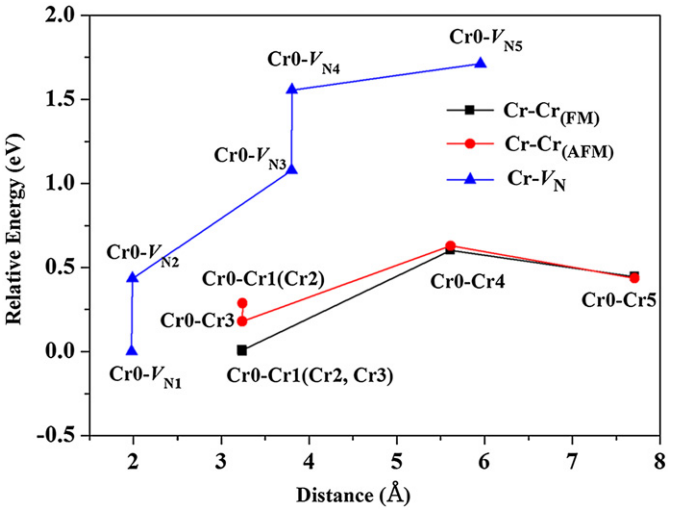

Fig. 2. Relative total energies of the Cr-doped GaN with N vacancies for different Cr-V_N distances (blue filled triangles), double Cr-doped GaN with ferromagnetic orientation for different Cr–Cr distances (red filled circles), and double Cr-doped GaN with antiferromagnetic orientation for different Cr–Cr distances (black filled squares). The three smallest total energies, corresponding to the nearest Cr-V_N, Cr–Cr pairs with ferromagnetic and antiferromagnetic orientation, are set to zero. (For interpretation of the references to color in this figure legend, the reader is referred to the web version of this article.)

3.2. *Vacancy-induced ferromagnetism ($Ga_{36}N_{36}+V_N$)*

We have first calculated the electronic structure and the induced magnetic moment of GaN with one N vacancy to know the states that will further hybridize with a Cr atom, so these results aid in analyzing and understanding the results for doped systems. GaN is a spin compensated semiconductor with the valence band consisting of N 2*p* states and Ga 4*s* states forming a well separated lowest conduction band. The introduction of one N vacancy removes N *sp* electrons and reorganizes the electron density of states, as shown in Fig. 3. Compared with the spin dependent total DOS of pure $Ga_{36}N_{36}$ in Fig. 3a, the spin-polarized electron density of states for $Ga_{36}N_{35}$ is seen in spin split, which implies that the N defect induces magnetism in this system. Such a half-metallic behavior is important for spintronic devices, and the same phenomenon could be seen in the following Cr-doped systems. In Table 1 we list the net spin values as well as the magnetic moments of the neighboring Ga and N for $Ga_{36}N_{35}$ system. It shows a total magnetic moment of 1.002 μ_B, and the Ga atoms surrounding the N defects contribute 0.639 μ_B, which are the main resource of the magnetism. The neighboring N atoms also provide an induced moment of 0.048 μ_B.

As is well known, the absence of an N atom introduces three shallow donor states in the system, leading to the imbalance in the two spin channels. These donor states are largely composed of the 4*s* and 4*p* orbitals of the four Ga atoms surrounding the N vacancy, as shown in Fig. 3d. Namely, each N vacancy generates four dangling bonds localized at the four Ga atoms surrounding the vacancy site. To investigate the nature of the electrons and spin exchange coupling between the Ga dangling bonds generated by N vacancy, we examine the isosurfaces of charge distribution of the donor levels in Fig. 4, in which the (a), (b), (c), and (d) correspond to i, ii, iii, and iv bands defined in Fig. 3b, respectively. The defect band through the Fermi level is mainly arising from Ga 4*s* states with a little contributions of Ga 4*p* and N *sp* states. When introducing one V_N, the charge of Ga atoms near V_N spreads toward the defect site through the dangling bonds, and the spin polarized interaction is so weak that opposing induced spins are created diffusely in a large space around the vacancy. The defect band ii indicates the single donor state, which is mainly located on the Ga atom situated along the *z*-axis above the vacancy site. The other two defect bands near the conduction band is mainly formed from a combination of dangling bonds of three equivalent Ga neighbors lying in plane with the vacancy. So the magnetic

Table 1
Formation energies (in eV), net spin values (in μ_B), magnetic moments (in μ_B) at the Cr and its neighboring Ga and N sites for the lowest energy structures. The moments arising out of Cr 3*d* orbitals are given in parentheses.

Configurations	Formation energy		Net spin *m*	m_{Cr} (μ^d)	m_{Ga}	m_N
	N-rich	N-poor				
$Ga_{36}N_{36}+V_N$	1.1	0.4	1.002		0.639	0.048
$CrGa_{35}N_{36}$	1.7		3.003	2.533 (2.415)	0.363	-0.092
$Cr_2Ga_{34}N_{36}$	3.4		5.998	Cr0: 2.944 (2.719) Cr1: 2.984 (2.757)	0.280	-0.326
$CrGa_{35}N_{36}+V_N$	5.3	4.6	4.000	3.607 (3.321)	0.320	-0.103
$CrGa_{35}N_{36}+N_T$	6.2	5.5				
$CrGa_{35}N_{36}+N_O$	6.7	5.9				

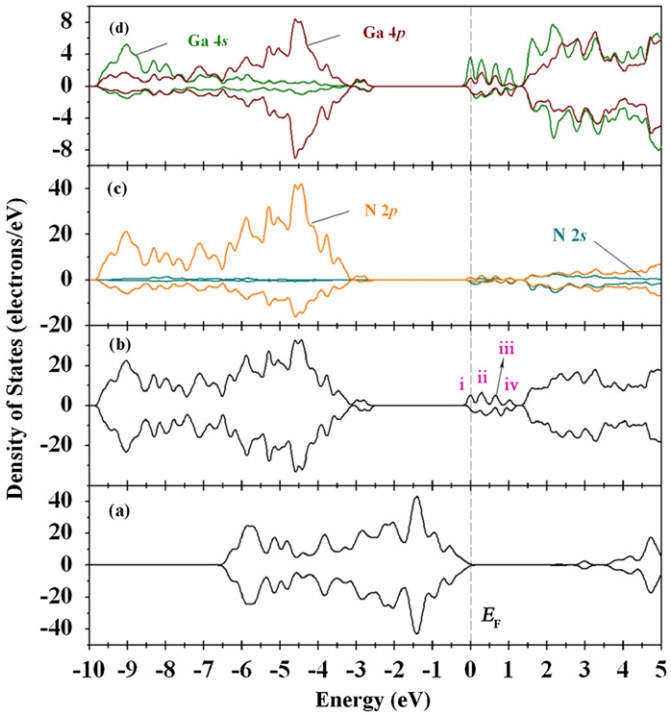

Fig. 3. Spin-dependent total (b) and partial DOSs (c,d) for $Ga_{36}N_{35}$ with pure $Ga_{36}N_{36}$ supercell (a) for comparison. The upper half for each panel is for majority spin and the other for minority spin.

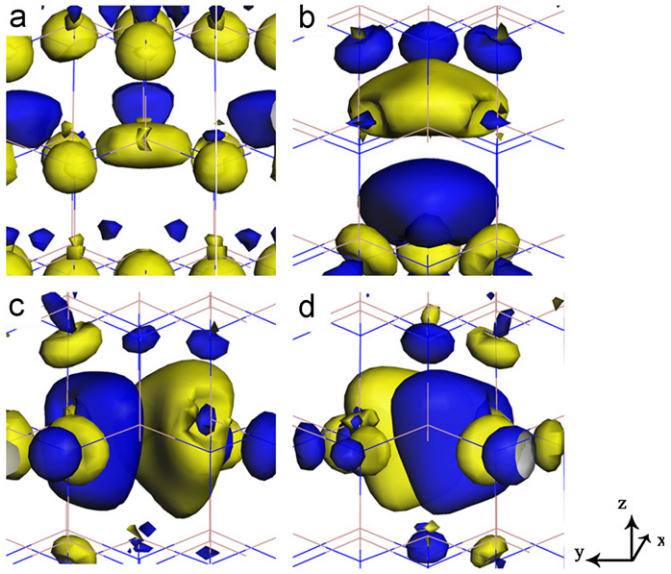

Fig. 4. Isosurfaces of charge distribution for i, ii, iii, and iv bands (corresponding to (a), (b), (c) and (d), respectively) of $Ga_{36}N_{35}$ defined in Fig. 3b.

moment in the system involved one V_N is mainly attributed to the Ga atoms due to the dangling bonds that create unpaired electrons, and the magnetic moments of Ga atoms decrease rapidly as the distance of Ga atoms from V_N increases.

3.3. *Ferromagnetism in pure Cr-doped systems ($CrGa_{35}N_{36}$ and $Cr_2Ga_{34}N_{36}$)*

It is known that the theoretical description of magnetic systems based on DFT requires some treatment of the self-interaction problem by using the DFT+U approach [32,33]. Therefore, the GGA and GGA+U methods are both used in the calculation of the $CrGa_{35}N_{36}$ configuration to test the performance of the on-site correlation by a Hubbard effective U term. Consider that the U parameter is applied to localized orbitals of specific atoms (normally the d or f levels of TM or rare-earth ions), we choose an effective interaction parameter U_{eff}=3.0 for Cr 3d electrons in our calculations that is based on an earlier paper [34]. The GGA approach is implemented in DMol^3 and the GGA+U approach is implemented in the CASTEP, so we first compare the results of the electronic band structures by using the GGA method in DMol^3 and Cambridge sequential total energy package (CASTEP) [35], respectively. As shown in their spin band structures in the Supporting information S1a and S1b, the valence band in DMol^3 is about 0.2 eV lower than that in CASTEP while the impurity bands near the Fermi level are almost the same. It indicates that the two codes do not make much difference on the electronic and magnetic properties by using both GGA methods. Now we compare the results at the level of GGA and GGA+U. From the DOS plots in Fig. 5, the Fermi level passes through the gap in the spin down DOS for both GGA and GGA+U methods and the system is half-metallic and ferromagnetic. It is clearly visible that the bands around Fermi level are mainly due to the presence of Cr impurity in the GaN host, which is in consistence with the fact that the Cr atom carries 84.3% (2.533 μ_B) of the total magnetic moment 3.003 μ_B, as shown in Table 1. Besides, the Cr atom induces antiferromagnetic polarizations of the neighboring N atoms with a small moment of -0.092 μ_B, which further lead to a 0.363 μ_B spin of the surrounding Ga atoms. This reflects the effect of through-bond spin polarization [36]. Three main impurity peaks can be seen from the GGA method in Fig. 5a, which are all mainly from the hybridization between Cr 3d and N 2p states. The GGA+U method improves the repulsion of the impurity bands, so the impurity band below the Fermi level splits into two, and those near the Fermi level become more separated (seen in S1c and Fig. 5b). However, we notice that in both calculations, the impurity levels mainly originates from the hybridization between Cr 3d and N 2p states with a small contribution of Ga sp states,

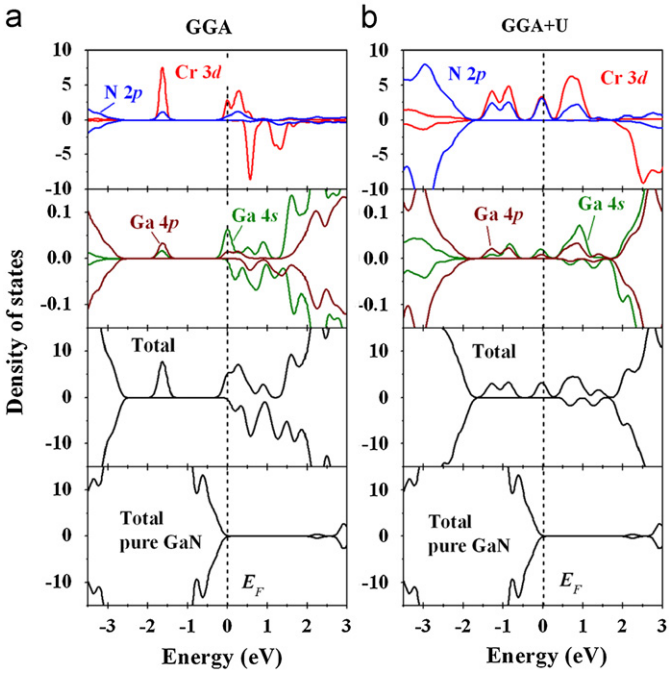

Fig. 5. Spin-dependent total and partial DOSs for $CrGa_{35}N_{36}$ by using GGA (a) and GGA+U (b) methods with pure $Ga_{36}N_{36}$ supercell for comparison. The upper half for each panel is for majority spin and the other for minority spin.

which are confirmed by the orbital analysis of the impurity bands. So we only give the isosurfaces of charge distribution for the three impurity bands for GGA approach in Fig. 6. It shows that all the three impurity peaks are contributed by the strong hybridization of Cr 3*d* (d_{xy} for band i, d_z2 for band ii and iii) and N 2*p* orbitals,

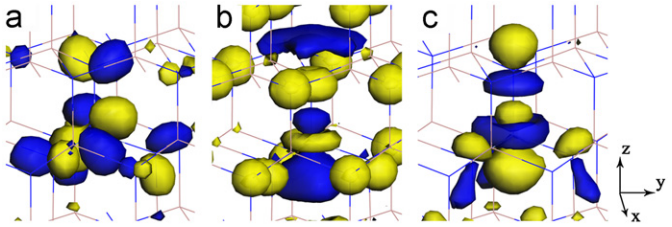

Fig. 6. Isosurfaces of charge distribution for i, ii, and iii bands (corresponding to (a), (b), and (c) respectively) of $CrGa_{35}N_{36}$ defined in Fig. 5b.

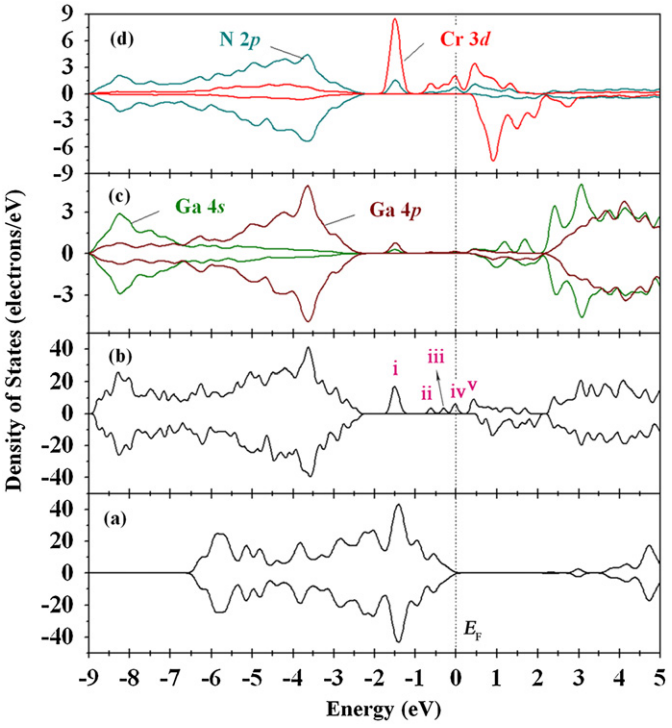

Fig. 7. Fig. 3 Spin-dependent total (b) and partial DOSs (c,d) for $Cr_2Ga_{34}N_{36}$ with pure $Ga_{36}N_{36}$ supercell (a) for comparison. The upper half for each panel is for majority spin and the other for minority spin.

forming π^* anti-bonding counterparts for the lower bands and σ^* anti-bonding state in the higher band. This result is consistent with the theory analysis that the $b_{2g}(d_{xy})$ and $e_g(d_{xz}, d_{yz})$ orbitals may hybridize strongly with N 2*p* orbitals in the valence bands, which consequently make the bonding states and anti-bonding counterparts [37]. Since the N 2*p* level is lower than the Cr 3*d* level, the ferromagnetic double exchange interaction is dominant in Cr-doped GaN. Contribution from the ferromagnetic double-exchange interaction is maximized when the anti-bonding states are partially occupied by electrons. Our GGA and GGA+U calculations prove that the GGA+U method only alter the repulsive interaction and the collective position of the electronic bands in this system. The results obtained by both methods are almost the same. The test conclusion is consistence with that in the recent calculation regarding to transition-metal-doped GaN [14]. Therefore, the results achieved at the level of GGA are given in the following study only.

The system of $Cr_2Ga_{34}N_{36}$ is also half-metallic and FM (Fig. 7). The Cr–Cr pair induce a magnetic moment of 5.998 μ_B, most of which originates from Cr 3*d* states (5.476 μ_B). The magnetic moments at two Cr sites (2.944 μ_B for Cr0 and 2.984 μ_B for Cr1) are slightly different because these atoms are not equivalent and have different Cr–N distances. For the case of Cr–Cr pair, the two Cr atoms are too far apart (3.027 Å) to allow significant direct overlap of the unpaired electron wave functions, thus instead of a substantial direct exchange mechanism, one can suggest a Cr–Cr indirect exchange interaction mediated by the N atom. This can be confirmed by the magnetic moment of $-0.326\ \mu_B$ for the mediated N atom as well as the overlap of N 2*p* and Cr 3*d* states especially in the majority orbitals of the DOSs. This is similar to what was found by Das et al. in their study of an ab initio cluster calculation on the ferromagnetism of the Cr-doped GaN [10]. As shown in the more intuitive isosurfaces of charge distribution (Fig. 8), The *p*–*d* hybridizations in the three filled bands (Figs. 8a–c) are mainly in the form of π^* anti-bonding states, and some σ^* anti-bonding states appear in the highest occupied level. And in the unfilled impurity band (Fig. 8e), the N atom, which simultaneously connects two Cr atoms, contributes its 2*p* states to involve in the π^* anti-bonding states with two d_{xz} orbitals. Differently, in Fig. 8c the two Cr d_{z^2} orbitals couple with each other to reduce the total energy, and this *d*–*d* hybridization is a good proof of the more delocalized Cr impurity bands in the DOS in comparison to single Cr doping. Moreover, the hybridization of N 2*p* and Cr 3*d* states is drastically reduced in double Cr-doped supercell. Hence, we can conclude that when the system has hole at the top of the *d* band, instead of *p*–*d* hybridization, it is the *d*–*d* spin coupling that stabilizes the ferromagnetic state. Therefore, the mechanism responsible for the FM coupling can be classified

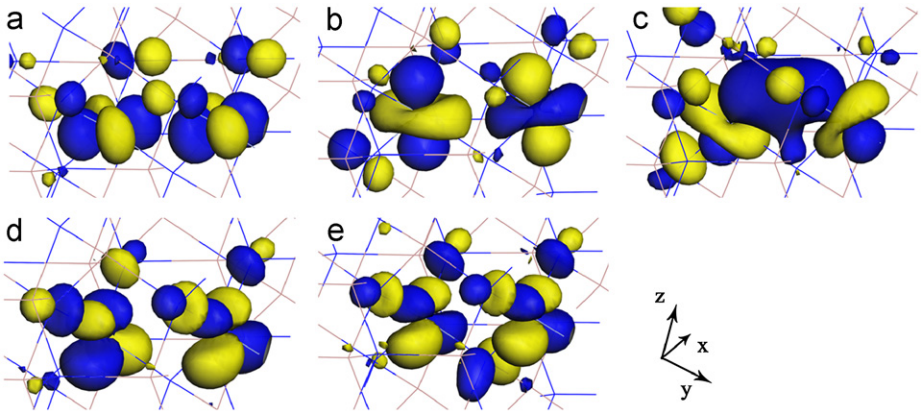

Fig. 8. Isosurfaces of charge distribution for i, ii, iii, iv and v bands (corresponding to (a), (b), (c), (d) and (e), respectively) of $Cr_2Ga_{34}N_{36}$ defined in Fig. 7b.

as the double exchange mechanism [38,39]. These results agree well with the conclusion from Tandon et al. where the authors reported a double exchange interaction in pure Cr-doped GaN system [9].

3.4. Ferromagnetism correlated with N vacancy ($CrGa_{35}N_{36}+V_N$)

Now we are focused on the electronic structure and spin coupling states of single Cr-doped GaN with one N vacancy. As seen in Table 1, One Cr+V_N complex contributes 4.000 μ_B to the total magnetic moment, and approximately 90% of the magnetic moment (3.607 μ_B) is arising from the Cr atom. This result is accordance with a recent report by Xu et al. in which they considered the existed N vacancies increase the magnetic moments of Cr-doped GaN [14]. The remaining spin is around the nearest Ga and N sites, and relative to that of Cr, the neighboring N atoms are also antiferromagnetic coupling with the Cr atom. It can be seen this through-bond spin polarization around the N vacancy is weaker because the unpaired spin is accommodated in the diffuse Ga 4*s*/4*p* orbitals through the Ga-dangling bonds.

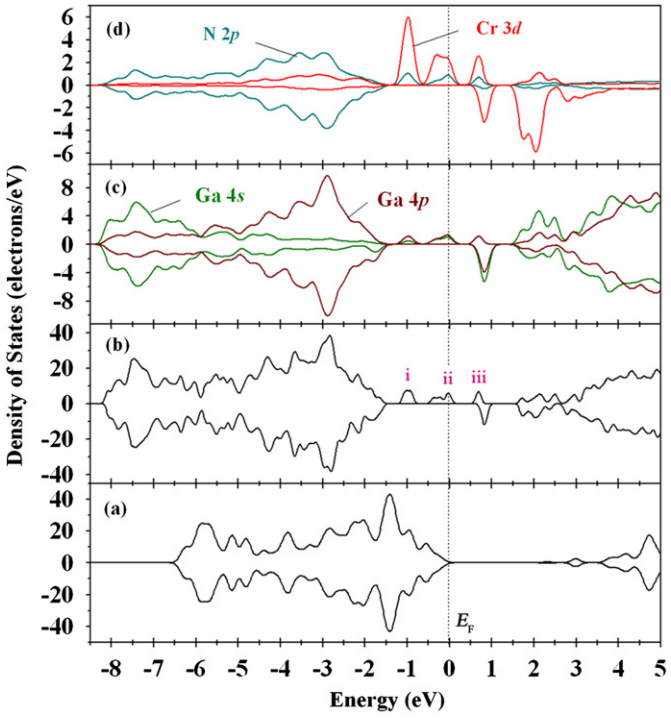

Fig. 9. Spin-dependent total (b) and partial DOSs (c,d) for $CrGa_{35}N_{35}$ with pure $Ga_{36}N_{36}$ supercell (a) for comparison. The upper half for each panel is for majority spin and the other for minority spin.

Fig. 9 demonstrates the total and partial DOS of $CrGa_{35}N_{35}$ system. As discussed above, for single Cr-doped GaN, the Cr atom has a d^3 configuration, and the empty Cr *d* states lie just below the conduction band edge while the partially filled Cr e_g states lie just below the t_{2g} levels. On the other hand, one N vacancy introduced into GaN releases three electrons, two of which form deep states just above the valance band edge with the other one forming near the bottom of the conduction band. When introducing one V_N in the Cr-doped GaN, the d^3 state forms somewhere in the middle of the gap, below the high-lying N vacancy state. The N vacancy provides an extra electron from this high-lying level to the Cr *d* states, and forms d^4, not d^3 electronic configuration for Cr in a Cr+V_N complex. The interaction of doped Cr and N vacancy makes the filled origination from the N vacancy move lower in energy, and together with the Fermi level.

The interaction of Cr *d* states with the N vacancy can be clearly seen in the isosurfaces of charge distribution in Fig. 10, in which (a), (b), and (c) correspond to the three impurity bands i, ii, and iii defined in Fig. 9b. The Cr 3*d* states, as the main origin of the magnetic moment of Cr atom, play important role in the impurity states around the Fermi level. We find that the electron clouds of Cr 3*d* states extend to the V_N site, and substantially hybridize with the N vacancy state, especially for the hole state above the Fermi level (as shown in Fig. 10c). The extension of Cr 3*d* orbital is benefit for the charge transfer from the N vacancy site to the neighboring Cr atom forming the Cr d^4 state. Combined with the DOS in Fig. 9, the Cr 3*d* electron states hybridize with the N 2*p* states in the valence band forming bonding states, and such hybridization interaction mediates the magnetic interactions [40]. The corresponding anti-bonding electronic states lie in the impurity gap, and are also arising from the strong hybridization of N 2*p* with Cr 3*d* states. Similarly, *p*–*d* π^* anti-bonding states are easily formed in the lower impurity bands, and the *p*–*d* σ^* anti-bonding states are the main hybridization in the higher impurity levels. It can clear be seen that in the Cr-doped GaN system, the introduction of N vacancy is beneficial to stabilize the ferromagnetic configuration and enhance the ferromagnetism.

It is reasonable to suppose that there coexist N vacancies, Cr atoms, and Cr+V_N complexes in the real samples and the fractional concentrations are dependent on synthesis [15,41]. Because of N pressure fluctuation during synthesis, a substitutional Cr and an N vacancy can be formed easily in different regions. This implies that some N-vacancy domains and some Cr-doping domains can be formed simultaneously in different regions separately. Because the Fermi level of the N vacancy is substantially higher than that of the Cr atom, the electron of the N vacancy must transfer to the Cr site and this electron transfer results in pairs of neutral Cr+V_N complex (the neuter is created by the Coulomb attraction). Just like discussed above, the N vacancy is in favor of the ferromagnetism through forming the Cr+V_N complex which contributes 4 μ_B to the

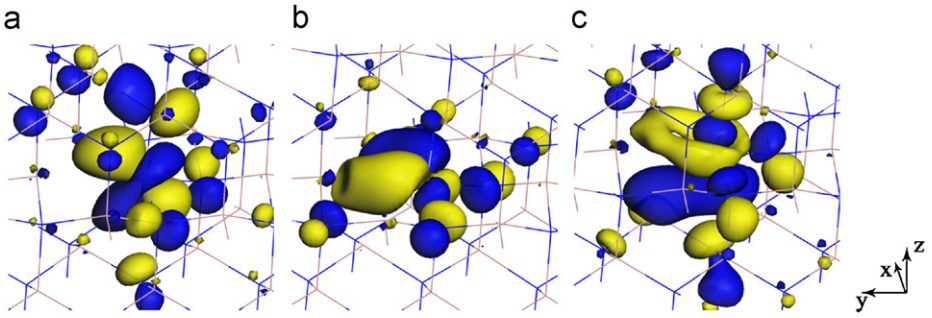

Fig. 10. Isosurfaces of charge distribution for i, ii, and iii bands (corresponding to (a), (b), and (c) respectively) of $CrGa_{35}N_{35}$ defined in Fig. 9b.

magnetic moment. On the other hand, the N vacancy can be harmful to the ferromagnetism through destroying the ferromagnetic spin coupling between two nearest substitutional Cr atoms. Therefore, when the Cr doping concentration is low, the N partial pressure should be controlled small to create an N-poor environment for Cr. In such condition, the impurity Cr atom will combine with the N vacancy to form Cr+V_N complex, and enhance the ferromagnetism. Conversely, when the Cr doping concentration is high, the Cr atoms will exist in the nearest neighbor form to reduce the total energy of the system. At this point, we should enhance the N partial pressure to reduce the appearance of N vacancy, avoiding the destruction of ferromagnetic coupling between the Cr atoms by the N vacancy.

4. Conclusion

In summary, we systematically investigated the nitrogen defects and their effect on the ferromagnetism in Cr-doped GaN by detailed first-principles calculations. We have studied the structural and electronic properties of one V_N, single Cr doping, double Cr doping, and single Cr doping with one N vacancy, indicating that the lowest energy arrangement for double Cr-doped (or Cr–V_N) GaN occurs when the Cr atoms (or the Cr and V_N) has the nearest distance. It has also been demonstrated that all the stable configurations involved are in ferromagnetism (FM) ground states. With the existence of one V_N only, the spin is mainly attributed to the nearest Ga atoms due to the dangling bonds that create unpaired electrons, and the magnetic moments of Ga atoms decrease rapidly as the distance of Ga atoms from V_N increases. For the case of single Cr doping, the magnetic moment at one Cr is 2.533 μ_B, and this is coupled antiferromagnetically to a small moment at the neighboring N sites. Strong ferromagnetism appears when introducing one Cr–Cr pair in a GaN supercell. Due to the strong *d*–*d* ferromagnetism coupling, these two Cr atoms occupied 99% of the total magnetic moment (5.998 μ_B). The FM coupling is mediated mainly by the N atom that connects the two Cr atoms, and a charge overlap between N 2*p* and Cr 3*d* states could be observed. The ferromagnetism is driven by a double exchange mechanism. The introduction of one V_N to the single Cr-doped system adds about 1 μ_B to the total magnetic moment (4.000 μ_B) by giving one extra electron to Cr. The electron clouds of Cr 3*d* states extend to the V_N site, and substantially hybridize with the N vacancy state. So in the Cr-doped GaN system, the introduction of N vacancy is beneficial to stabilize the ferromagnetic configuration and enhance the ferromagnetism. Therefore, when the Cr doping concentration is low, the N partial pressure should be controlled small to create an N-poor environment, so the N vacancy in the samples will combine with impurity Cr to form Cr+V_N complex, enhancing the ferromagnetism. Conversely, when the Cr doping concentration is high, we should enhance the N partial pressure to reduce the destruction of ferromagnetic coupling between the Cr atoms by the N vacancy.

Supplementary material available

Electronic band structures of $CrGa_{35}N_{36}$ by using GGA functional in DMol[3] and CASTEP codes as well as the GGA+U result in CASTEP. This material is available free of charge via the Internet at http://www.sciencedirect.com.

Acknowledgments

This work is supported by the National Natural Science Foundation of China (Grant nos. 50802056 and 50721002), 973 Program of China under Grant no. 2009CB930103, Natural Science Foundation of Shandong Province of China under Grant no.Y2007B08, the Specialized Research Fund for the Doctoral Program of Higher Education of China under Grant no. 20070422060, Youth Scientist (Doctoral) Foundation of Shandong Province of China under Grant no. BS2009CL038, and the Independent Innovation Foundation of Shandong University (IIFSDU) under Grant no. 2009TS016.

Appendix A. Supplementary material

Supplementary data associated with this article can be found in the online version at doi:10.1016/j.jssc.2010.08.038.

References

[1] H. Ohno, Science 281 (1998) 951.
[2] T. Dietl, H. Ohno, F. Matsukura, J. Cibert, D. Ferrand, Science 287 (2000) 1019.
[3] J.M.D. Coey, Curr. Opin. Solid State Mater. Sci. 10 (2006) 83.
[4] J. Kudrnovsky, I. Turek, V. Drchal, F. Maca, P. Weinberger, P. Bruno, Phys. Rev. B 69 (2004) 115208.
[5] K. Sato, P.H. Dederichs, K. Araki, H. Katayama-Yoshida, Phys. Status Solidi (c) 7 (2003) 2855.
[6] Q. Wang, Q. Sun, P. Jena, Nano Lett. 5 (2005) 1587.
[7] S.E. Park, H.–J. Lee, Y.C. Cho, S.–Y. Jeong, C.R. Cho, S. Cho, Appl. Phys. Lett. 80 (2002) 4187.
[8] M. Hashomoto, Y.–K. Zhou, M. Kanamura, H. Asahi, Solid State Commun. 122 (2002) 37.
[9] N. Tandon, G.P. Das, A. Kshirsagar, Phys. Rev. B 77 (2008) 205206.
[10] G.P. Das, B.K. Rao, P. Jena, Phys. Rev. B 69 (2004) 214422.
[11] X.Y. Cui, J.E. Medvedeva, B. Delley, A.J. Freeman, N. Newman, C. Stampfl, Phys. Rev. Lett. 95 (2005) 256404.
[12] Stephen Y. Wu, N. Newman, Appl. Phys. Lett. 89 (2006) 142105.
[13] X.Y. Cui, J.E. Medvedeva, B. Delley, A.J. Freeman, C. Stampfl, Phys. Rev. B 75 (2007) 155205.
[14] B. Xu, B.C. Pan, J. Appl. Phys. 105 (2009) 103710.
[15] H.X. Liu, Stephen Y. Wu, R.K. Singh, L. Gu, David J. Smith, N. Newman, Appl. Phys. Lett. 85 (2004) 4076.
[16] C.G. Van de Walle, J. Neugebauer, J. Appl. Phys. 95 (2004) 3851.
[17] H.P. Maruska, J.J. Tietjen, Appl. Phys. Lett. 15 (1969) 327.
[18] P. Perlin, T. Suski, H. Teisseyre, M. Leszczynski, I. Grzegory, J. Jun, S. Porowski, P. Boguslawski, J. Bernholc, J.C. Chervin, A. Polian, T.D. Moustakas, Phys. Rev. Lett. 75 (1995) 296.
[19] T. Mattila, R.M. Nieminen, Phys. Rev. B 55 (1997) 9571.
[20] K. Saarinen, T. Laine, S. Kuisma, J. Nissilä, P. Hautojärvi, L. Dobrzynski, J.M. Baranowski, K. Pakula, R. Stepniewski, M. Wojdak, A. Wysmolek, T. Suski, M. Leszczynski, I. Grzegory, S. Porowski, Phys. Rev. Lett. 79 (1997) 3030.
[21] J. Oila, V. Ranki, J. Kivioja, K. Saarinen, P. Hautojärvi, J. Likonen, J.M. Baranowski, K. Pakula, T. Suski, M. Leszczynski, I. Grzegory, Phys. Rev. B 63 (2001) 045205.
[22] K. Saarinen, T. Suski, I. Grzegory, D.C. Look, Phys. Rev. B 64 (2001) 233201.
[23] H. Jin, Y. Dai, B.B. Huang, M.–H. Whangbo, Appl. Phys. Lett. 94 (2009) 162505.
[24] M.G. Ganchenkova, R.M. Nieminen, Phys. Rev. Lett. 96 (2006) 196402.
[25] E. Kaxiras, in: Atomic and Electronic Structure of Solids, Cambridge University, Cambridge, England, 2003.
[26] B. Delley, J. Chem. Phys. 92 (1990) 508;
B. Delley, J. Quantum Chem. 69 (1998) 423.
[27] J.P. Perdew, Y. Wang, Phys. Rev. B 45 (1992) 13244.
[28] H.J. Monkhorst, J. Pack, Phys. Rev. B 13 (1976) 5188.
[29] H. Schulz, K.H. Thiemann, Solid State Commun. 23 (1977) 815.
[30] B. Sanyal, S. Mirbt, J. Magn. Magn. Mater. 290-291 (2005) 1408.
[31] J. Wang, P. Chen, X. Guo, Z. Li, W. Lu, J. Cryst. Growth 275 (2005) 393.
[32] R.L. Martin, F. Illas, Phys. Rev. Lett. 79 (1997) 1539.
[33] V.I. Anisimov, J. Zaanen, O.K. Andersen, Phys. Rev. B 44 (1991) 943.
[34] K.S. Yang, Y. Dai, B.B. Huang, Chem. Phys. Chem. 10 (2009) 2327.
[35] M. Segall, P. Lindan, M. Probert, C. Pickard, P. Hasnip, S. Clark, M. Payne, J. Phys. Condens. Matter 14 (2002) 2717.
[36] K. Yoshizawa, T. Kuga, T. Sato, M. Hatanaka, K. Tanaka, T. Yamabe, Bull. Chem. Soc. Jpn. 69 (1996) 3443 and references therein.
[37] N. Tandon, G.P. Das, A. Kshirsagar, J. Phys. Condens. Matter 18 (2006) 9245.
[38] K. Sato, P.H. Dederichs, H. Katayama-Yoshida, J. Kudrnovsky, Physica B 340-342 (2003) 863.
[39] K. Sato, P.H. Dederics, H. Katayama-Yoshida, Europhys. Lett. 61 (2003) 403.
[40] M.H.F. Sluiter, Y. Kawazoe, P. Sharma, A. Inoue, R Raju., A, C. Rout, U.V. Waghmare, Phys. Rev. Lett. 94 (2005) 187204.
[41] L. Gu, S.Y. Wu, H.X. Liu, R.K. Singh, N. Newman, D.J. Smith, J. Magn. Magn. Mater. 290-191 (2005) 1395.